Instrumented indentation study of plastic deformation in bulk metallic glasses

W.H. Li
Institute of Materials, Shanghai University, Shanghai 200072, People's Republic of China

T.H. Zhang and D.M. Xing
State Key Laboratory of Nonlinear Mechanics, Institute of Mechanics, Chinese Academy of Sciences, Beijing 100080, People's Republic of China

B.C. Wei[a] and Y.R. Wang
National Microgravity Laboratory, Institute of Mechanics, Chinese Academy of Sciences, Beijing 100080, People's Republic of China

Y.D. Dong
Institute of Materials, Shanghai University, Shanghai 200072, People's Republic of China

(Received 6 February 2005; accepted 28 June 2005)

Mechanical properties and micro-plastic deformation behavior of five bulk metallic glasses (BMGs) were studied by instrumented indentation. These materials included $La_{60}Al_{10}Ni_{10}Cu_{20}$, $Mg_{65}Cu_{25}Gd_{10}$, $Zr_{52.5}Al_{10}Ni_{10}Cu_{15}Be_{12.5}$, $Cu_{60}Zr_{20}Hf_{10}Ti_{10}$, and $Ni_{60}Nb_{37}Sn_3$ alloys. Remarkable difference in deformation behavior was found in the load–displacement curves of nanoindentation and pileup morphologies around the indents. Serrated plastic deformation depended on the loading rate was found in Mg-, Zr-, and Cu-based BMGs. The subsurface plastic deformation zone of typical alloys was investigated through bonded interface technique using depth-sensing microindentation. Large and widely spaced shear bands were observed in Mg-based BMG. The effect of loading rate on the indentation deformation behaviors in different BMGs was elucidated by the change of shear band pattern.

I. INTRODUCTION

Although bulk metallic glasses (BMGs) have shown potential as structural materials due to their high strength, high hardness, good wear resistance, excellent elasticity, and easily forming in viscous state, applications are currently limited by the lack of any significant plastic deformation at room temperature. Understanding the micro-mechanisms of plastic deformation and developing the constitutive relationships for BMGs is an active area of research.[1–7] As an excellent tool to determine mechanical properties on a local scale, nanoindentation has been intensively studied in the thin film and nanocrystals material.[8–10] Recently, nanoindentation has been proposed as a key method for the study of localized deformation by shear banding in BMGs.[5,11–17] A growing number of authors have considered the formation of individual shear bands by nanoindentation, where displacement bursts in the Load-displacement (P-h) response have been correlated with discrete shear banding events.[12,14] It is found that the character of serrated flow depends strongly on the composition and structure of BMGs, as well as the applied strain rate during nanoindentation measurements.[12–14,17] The Pd-based alloys exhibit sharper displacement bursts than for Zr-based materials at the same loading rate.[12] Schuh et al. constituted a new high-rate regime of homogeneous flow on the deformation map of metallic glasses.[5,12,13] They suggest that there is a transition in plastic flow behavior in which serrations are suppressed at higher strain rate. On the other hand, it is well established that higher strain rate promotes inhomogeneous, not homogeneous, flow.[18–20] To conclusively determine the formation and the progress of shear bands, more direct observations are needed. In the present work, the mechanical properties and the plastic deformation behavior in Mg-, La-, Zr-, Cu-, and Ni-based bulk metallic glasses were investigated by using nanoindentation. The subsurface deformation morphology of different BMGs was studied by using depth-sensing microindentation through the bonded interface technique.[21] The effect of the loading rate on the shear bands pattern is also studied.

II. EXPERIMENTAL

Five BMG were studied, including $La_{60}Al_{10}Ni_{10}Cu_{20}$, $Mg_{65}Cu_{25}Gd_{10}$, $Zr_{52.5}Al_{10}Ni_{10}Cu_{15}Be_{12.5}$, $Cu_{60}Zr_{20}Hf_{10}Ti_{10}$, and $Ni_{60}Nb_{37}Sn_3$. Cylindrical rods

[a]Address all correspondence to this author.
e-mail: weibc@imech.ac.cn
DOI: 10.1557/JMR.2006.0037

3 mm in diameter of La-, Zr-, Cu-, and Ni-based BMG were prepared by melting pure metals in an argon atmosphere and then chill-casting in a copper mold. The $Mg_{65}Cu_{25}Gd_{10}$ alloy was processed by melting pure Mg with intermediate Cu–Gd alloy and then chill-casting in a copper mold with the inner diameter of 5 mm. The structure of the samples was characterized by x-ray diffraction (XRD) in a Philips PW 1050 diffractometer (Eindhoven, The Netherlands) using Cu K_α radiation. The specimens for nanoindentation measurements were mechanically polished to a mirror finish and tested in a MTS Nano Indenter XP (Oak Ridge, TN) with a Berkovich diamond tip (tip radius is about 50 nm). Fused silica was used as a reference sample for the initial tip calibration procedure. The indentations were performed in load-control mode to a depth limit of 1 μm using loading rates from 0.075 to 5 mN/s. The maximum load was held constant for 10 s and then was unloaded at the rates as same as the loading one. The thermal drift of the instrument was maintained below 0.05 nm/s. At least six indentations were made for each test. All tests were carried out at 23 °C. The study of subsurface deformation morphology was obtained through the bonded interface technique.[21] The two mirror polished surfaces were bonded using a high strength adhesive. A careful bonding was made to minimize the bond layer thickness and ensuring the bonded layer thickness for different specimen is almost same. The micro-indentation tests were performed with Vickers indenter on the bonded interface as well as away from it. The indenter is attached to a load cell that is bolted to the bottom of the crosshead of an Instron 5848 Microforce Tester (Canton, MA). The indentation measurements were performed in displacement-control mode to a load limit of 10 N. It was also ensured that one of the indentation diagonal coincides with the interface. The displacement between the two crossheads was recorded. The hardness and modulus of elasticity were obtained from the nanoindnetation curves using the Oliver–Pharr method.[22] These values were calibrated by a pure aluminum sample. Indents surface and subsurface observations were performed by a JSM-6460 scanning electron microscope (SEM, Tokyo, Japan) and a Neophot-21 optical microscope. The uniaxial compression tests on cylindrical samples of 3 mm in diameter and 5.8 mm in length were performed in a commercial Instron-type testing machine at room temperature. The crosshead was moved at a constant speed with an initial strain rate of 1.0×10^{-4} s^{-1}.

III. RESULTS AND DISCUSSION

Figure 1 shows the XRD patterns of as-cast samples of composition $La_{60}Al_{10}Ni_{10}Cu_{20}$, $Mg_{65}Cu_{25}Gd_{10}$, $Zr_{52.5}Al_{10}Ni_{10}Cu_{15}Be_{12.5}$, $Cu_{60}Zr_{20}Hf_{10}Ti_{10}$, and $Ni_{60}Nb_{37}Sn_3$. All as-cast alloys exhibit an XRD spectrum typical for amorphous phase.

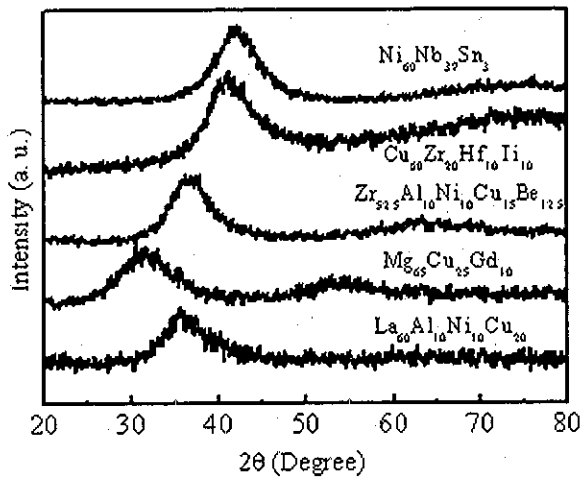

FIG. 1. XRD patterns for five BMG alloys.

Typical load-displacement (P-h) curves for nanoindentations on each of the five amorphous alloys are presented in Fig. 2(a), where the BMGs are indented to the depth of 1000 nm at a constant loading rate of 1 mN/s. The hardness (H) and modulus of elasticity (E) values of each alloys determined from nanoindentation measurements are listed in Table I. The Ni-based BMG shows the

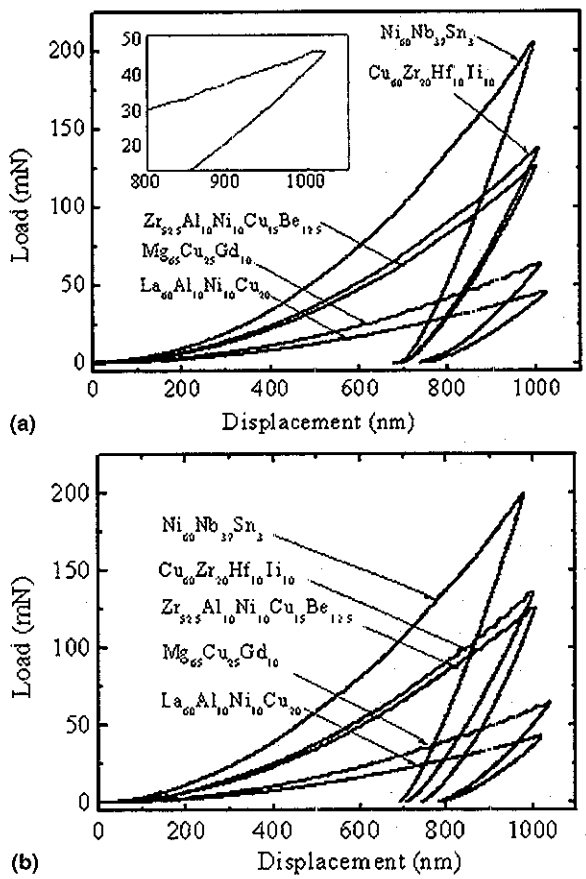

FIG. 2. Typical load-displacement (P-h) curves during nanoindentations at the loading rate of (a) 1 mN/s and (b) 0.075 mN/s for five BMGs.

TABLE I. Mechanical parameters and glass transition temperature T_g of five BMGs.

Alloy system	H^1 (GPa)	H^2 (GPa)	E (GPa)	σ_y (MPa)	T_g (K)	T/T_g
$La_{60}Al_{10}Ni_{10}Cu_{20}$	2.0	2.2	49.7	544	402	0.736
$Mg_{65}Cu_{25}Gd_{10}$	2.4	2.7	65.4	650	409	0.724
$Zr_{52.5}Al_{10}Ni_{10}Cu_{15}Be_{12.5}$	5.3	7.0	118.8	1960	685	0.432
$Cu_{60}Zr_{20}Hf_{10}Ti_{10}$	6.1	7.5	131.1	2100	722	0.410
$Ni_{60}Nb_{37}Sn_3$	8.8	10.9	217.2	3200	895	0.331

H^1: Vickers hardness; H^2: nanoindentation hardness; T: room temperature

highest hardness and modulus of 10.9 and 217.2 GPa, respectively, while the La-based BMG shows the lowest hardness and modulus of 2.2 and 49.7 GPa, respectively. The compressive strength of each BMGs studied here was measured using uniaxial compression tests at an initial strain rate of 1.0×10^{-4} s^{-1}. The yield strength and hardness values measured by conventional Vickers hardness tests are also listed in Table I.

The yield strength of a material under compression is related to the hardness determined from indentation according to[23]

$$H = K\sigma_y \quad , \tag{1}$$

where σ_y is the yield stress, H is the hardness, and the constrain factor K depends on the indenter shape, the depth of indentation as well as the strain-hardening characteristics. Figure 3 exhibits the relationship of five BMGs between H (including nanoindentation hardness and Vickers hardness) and σ_y. The values of Vickers microhardness are smaller than the corresponding hardness determined from nanoindentation. The value of $K \sim 3$ is a good approximation for a variety of classical glass-forming alloys as well as BMGs.[5] The value of K for the present five BMGs is about 2.7 for Vickers hardness, whereas about 3.4 for nanoindentation with Berkovich tip.

From the loading curves in Fig. 2(a), it can be found that Mg-based BMG exhibits the most prominent serrated flow at the loading rate of 1 mN/s, while Zr-, Cu-, Ni-, and La-based BMGs do not exhibit distinct serrated flow behavior during the loading period. In addition, it also can be seen that during the hold segment for 10 s at the maximum load, a creep displacement of about 20 nm is clearly observed in the inset of Fig. 2(a) for the La-based BMG, while no creep deformation is found for the other four BMGs. The loading curves for five BMG alloys at the loading rate of 0.075 mN/s are shown in Fig. 2(b). It can be seen that at this low loading rate, Mg- and Cu- based BMG exhibit the most prominent serrated flow, and Zr-based BMG exhibits the less prominent serrated flow. In contrast, La- and Ni-based BMGs show almost no discrete steps during the loading process. The deformation behavior during nanoindentation in the present Zr-based BMG agrees well with that of other Zr-based BMGs with similar chemical composition, in which a less prominent serrated flow was observed at low loading rates.[5,12] However, an obvious serrated flow was shown in the La–25Al–10Cu–5Ni–5Co BMG at the loading rate of 0.8 mN/s.[13] This difference is due to that the T_g of the present alloy is 80 K lower than that of the former one, as well as the change of local atomic structure, though the chemical composition has only a slight difference.[24]

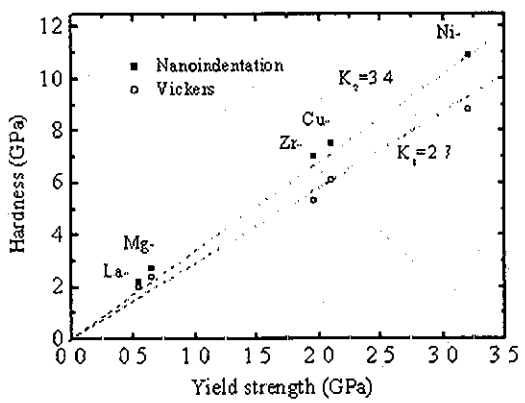

FIG. 3. The relationship between hardness (H) and yield strength (σ_y) for five BMGs.

In crystalline alloys, the physical basis for the appearance of serrated flow is the negative strain rate sensitivity originating mainly from the interaction between mobile dislocations and diffusing solute atoms.[25] In the case of BMGs, being noncrystalline materials, the mechanism of the appearance of instability steps must be different. It was well known from earlier work that plastic deformation in metallic glasses at room temperature is concentrated into narrow regions called shear bands.[18–20] Serrated flow phenomenon manifested as a stepped load–displacement curve punctuated by discrete bursts of plasticity during nanoindentation was already found in Pd-, Zr-, and Nd-based BMGs.[5,12–14,16] The discrete steps correspond to the activation of individual shear bands. It should be noted that the discrete steps in the load–displacement curves in BMGs caused by the nucleation and propagation of shear bands is much smaller than the pop-ins in crystalline materials caused by the dislocation bursts. From the Fig. 2, it can be seen that the plastic deformation behavior of the five BMG alloys exhibits quite different feature under nanoindentation measurements. This implies that the formation and propagation of shear bands during plastic deformation are in different modes. There is a general trend for metallic glass that, as the testing temperature approaches T_g ($T/T_g > 0.7$), the deformation behavior changes gradually from inhomogeneous to homogenous viscous flow.[20] The T/T_g values of the BMGs in this study spread out in a quite wide range (from 0.331 to 0.736 as given in Table I). However, the deformation behavior of the five BMGs (Fig. 2) does not show a distinct trend with changing of T/T_g values. Ni- and La-based BMGs with the

highest and the lowest T/T_g value, respectively (0.736 and 0.331), exhibit a continuous plastic deformation without obvious discrete steps at the loading rate range from 0.075 to 1.0 mN/s, and Zr- and Cu-based BMGs with medium T/T_g values, show a distinct serrated flow at the low loading rate. However, the Mg-based BMG with a large T/T_g value of 0.724 exhibits the most pronounced serrated flow even at the high loading rate. The serrated flow behavior also does not depend upon the mechanical parameters, such as hardness and modulus of elasticity (Table I), as the second softest Mg-based BMG exhibits the most discrete plastic deformation. This suggests that the local atomic arrangements and compositions near the shear bands may play an important role in the formation and propagation of shear bands.

Typical surface morphologies of indents for the five BMGs after indentation at the loading rate of 1.0 mN/s are shown in Fig. 4. It reveals two kinds of surface deformation features for the present alloys. A number of incomplete circular patterns of shear bands were observed in the pile-up area around the indents for $Mg_{65}Cu_{25}Gd_{10}$, $Cu_{60}Zr_{20}Hf_{10}Ti_{10}$, and $Ni_{60}Nb_{37}Sn_3$ BMGs. They represent overlapping layers of displaced material that flow upwards and away from the depth of the indents. The other type of alloys such as $La_{60}Al_{10}Ni_{10}Cu_{20}$ and $Zr_{52.5}Al_{10}Ni_{10}Cu_{15}Be_{12.5}$ do not exhibit distinct shear bands surrounding the indents, though the serrated flow is observed in the loading curve of $Zr_{52.5}Al_{10}Ni_{10}Cu_{15}Be_{12.5}$ in Fig. 2. Therefore, it is interesting to study the shear band patterns under the indents for clarify the deformation behavior in different alloy systems.

The deformation regions underneath indents are investigated for two typical alloys, i.e., Zr-based BMG, which shows less pronounced serrated flow in loading curve [Fig. 2(a)] and no shear bands on the surface of the specimens after indentation (Fig. 4), and Mg-based BMG, which exhibits the most pronounced discrete steps in nanoindentation measurements (Fig. 2) and a number of shear bands around the indents (Fig. 4). Figure 5(a) shows deformation region underneath a Vickers indenter for the Zr-based BMG with the indentation rate of 1000 nm/s, obtained by employing the bonded interface technique. Though no obvious serrated flow in the *P-h* curve (Fig. 2) and no shear bands near the indent after indentation (Fig. 4) were observed, a distinct inhomogeneous deformation feature characterized by forming shear bands is exhibited. The deformation zone is semicircular in nature containing two types of shear bands; those are semi-circular and radial shear bands. The density of radial shear band is considerably larger than that of the radial one. The spacing between the semicircle shear bands exhibits less dependence on the distance from the indenter tip. The flow line feature exhibited by atomic force microscopy studies confirmed that these are shear bands other than cracks. The morphology of the shear band pattern is similar to that seen in the Pd-based BMG, though the applied load and loading rate are much lower in the present case [26,27]. It should be noted that a large number of semi-circular shear bands form in the deformation zone underneath the tip, but they do not propagate to the upper surface of the specimen. Figure 5(b) shows morphology of subsurface deformation in the Mg-based BMG with the indentation rate of 1000 nm/s. The approximative semicircular and radial shear bands are observed. Each semicircular shear band is intersected by a number of radial shear bands. The density of shear band in the deformation zone of Mg-based BMG is much smaller than that in the Zr-based BMG, whereas, the thickness of each shear band in is larger in the former BMG. Moreover, the spacing between shear bands (both for the semicircular and radial shear bands) in Mg-based

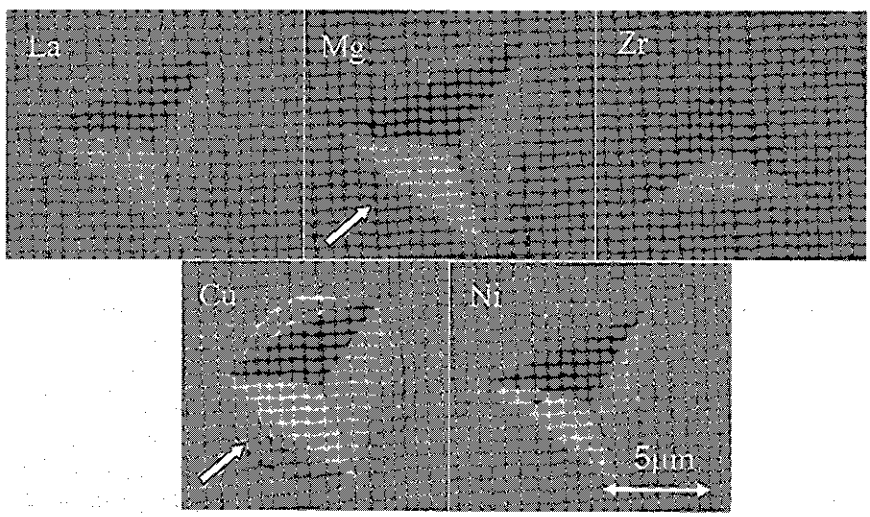

FIG. 4. SEM images of evolved deformation features after nanoindentation at the loading rate of 1 mN/s for five BMGs. Localized plastic flow was marked with arrows.

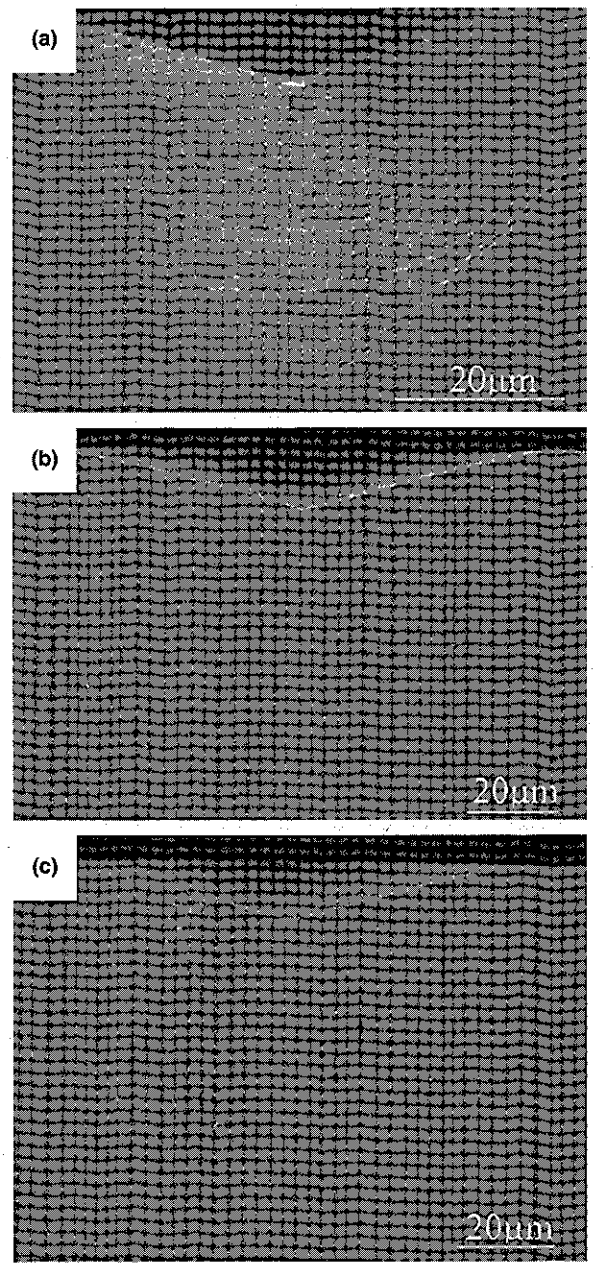

FIG 5. SEM images of the deformation region underneath a Vickers indenter for (a) $Zr_{52.5}Al_{10}Ni_{10}Cu_{15}Be_{12.5}$ BMG with the loading rate of 1000 nm/s, (b) $Mg_{65}Cu_{25}Gd_{10}$ BMG with the loading rate of 1000 nm/s and (c) $Mg_{65}Cu_{25}Gd_{10}$ BMG with the loading rate of 15 nm/s

BMG is larger and shows a successive increase with increasing the distance from the indenter tip. Another distinct feature for the shear band pattern in Mg-based BMG underneath the tip is that the semicircular shear bands propagate to the upper surface of the sample

More recently, Ramamurty and coworker have used the bonded interface technique to reveal the shear band pattern through Vickers indentation.[24 26 27] They proved that, the bonded interface technique is likely closer to a plane-stress than a plane-strain stress state owing to the weak interfacial layer beneath the indenter. The semicircular shear bands are surface steps created due to the outward plastic flow of material into the compliant adhesive layer (out-of-plane displacement), while the radial shear bands accommodate the true indentation strain (in-plane displacement). Depending on the relative constraint experienced by the material for its plastic flow into the bonded interface, one type of morphology dominates over the other in appearance More the constraint at the interface, more pronounced will be the radial shear bands Although the semicircular shear bands do not accommodate the in-plane displacement, they do reflect the plastic deformation characters of the material itself. Therefore, the shear band patterns underneath the indents shown above can qualitatively interpret the deformation behavior of the alloys during nanoindentation measurements. The plastic deformation in the Mg-based alloy occurs by thick shear bands with relative large spacing. This gives rise to the pronounced discrete steps in the loading curve, though the T/T_g value is high, whereas in the Zr-based BMG the simultaneous operation of multiple shear bands with a small thickness leads to a relatively continuous plastic deformation. It should be pointed that another reason may also play an important role in the change of deformation mode That is the propagation of the semicircular shear bands underneath the indents. The propagation process of shear bands is determined by the local atomic arrangements and compositions near the shear bands. The different shear bands pattern shown in Fig. 5 indicates that the Zr-based BMG has a higher resistance on the operation of shear bands, which is consistent with the reported much higher toughness in Zr-based BMGs than that in Mg-based BMG.[28] This should also be the reason for the absence of shear bands near the indent for Zr-based BMG after indentation (Fig. 4)

The effect of the indentation loading rate on the deformation behavior of the BMGs was also studied. La- and Ni-based BMGs do not show distinct discrete steps during the loading process in loading rate range from 0.075 to 1.0 mN/s [Figs. 2(a) and 2(b)] The loading portions of typical load–displacement curves at different loading rates for Mg- and Zr-based BMG are shown in Fig. 6. The origin of each curve has been displaced for clearer observation It can be seen that the serrated flow phenomenon for $Mg_{65}Cu_{25}Gd_{10}$ [Fig. 6(a)] and $Zr_{52.5}Al_{10}Ni_{10}Cu_{15}Be_{12.5}$ [Fig 6(b)] BMGs is strongly dependent on the indentation loading rate. A low indentation rate promotes more pronounced serrations, and rapid indentation suppresses serrated flow for both BMGs. The critical loading rate for this transition is about 5 mN/s for the Mg-based BMG, 0.075 mN/s for Zr-based BMG, and 0.5 mN/s for Cu-based BMG. This trend of serrated flow phenomenon changing with indentation rates has also been observed in a variety of other

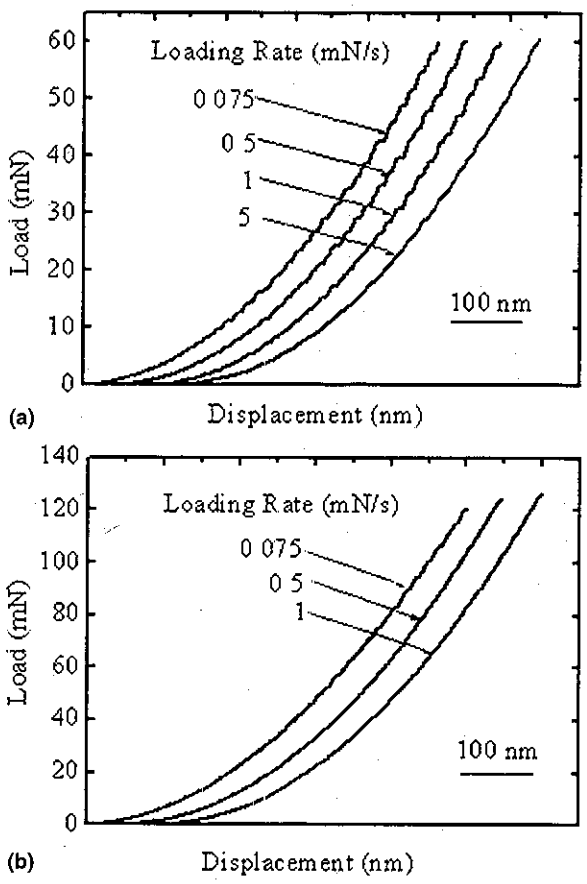

FIG 6 Loading portions of typical load-displacement (*P-h*) curves during nanoindentation measured on at different loading rates for (a) $Mg_{65}Cu_{25}Gd_{10}$ BMG and (b) $Zr_{52.5}Al_{10}Ni_{10}Cu_{15}Be_{12.5}$ BMG Curves are offset from origin for clear viewing

BMGs, including Pd-, La-, and Be-free Zr-based BMGs.[5,12–14,17] Schuh et al. proposed that, these results represent a transition from deformation being carried by a single shear band at low rates, to the simultaneous operation of multiple shear bands at higher rates.[12,13,17]

The shear band pattern in the deformation zone underneath the indent was also investigated. A typical optical morphology for the Mg-based BMG at a low penetration rate of 15 nm/s is shown in Fig. 5(c). A decreased shear band density and increased shear bands thickness [for both semi-circular and radial shear bands, Figs. 5(b) and 5(c)] are observed at the loading rate of 15 nm/s compared with that at 1000 nm/s. This proves that higher loading rate will promote the simultaneous operation of multiple shear bands. The inter-band spacing and the thickness of shear bands are found to increase significantly from the indenter tip region to the deeper region. It is conceivable that the strain rate decreases gradually during the indentation process.[15] This further proves that at low loading rate the individual shear band propagated rapidly and accommodate the applied strain, leading to a strain burst. The observation of the change of shear band spacing and shear band thickness with the penetration depth consists with the feature of the loading curves in Mg-based BMG [Figs. 2 and 6(a)], where the size of each step increases significantly with the penetration depth. While for the Zr-based BMG the shear band spacing exhibits less dependence on the penetration depth [Fig. 5(a)]. This implies that the shear band feature is relatively not sensitive to the loading rate in Zr-based BMG. Moreover, the plastic deformation zone for the high rate indented specimen [Fig. 5(b)] is larger than that in the low rate one [Fig. 5(c)]. This means that the strain caused by the form of shear bands is accommodated in larger volume of surrounding material. The enlarged strain field and the simultaneous operation of shear bands contribute to a continuous loading curve during nanoindentation at the high loading rate.

The characters of shear bands, e.g., interband spacing and thickness, differ in different alloy system at the same loading rate. As seen in Figs. 5(a) and 5(b), Mg-based BMG exhibits a larger shear band spacing and shear band thickness than that in Zr-based BMG. This should be the reason that the critical loading rate for the disappearance of prominent serrated flow is much higher in the Mg-based BMG than that in Zr-based BMG. A high density of shear bands is also formed in the Cu-based BMG, as numerous shear bands can clearly be found on the surface of specimen around the indent (Fig. 4). The operation of many shear bands ceases the serrated flow during indentation at the high loading rate [Fig. 2(a)].

IV. SUMMARY

Mechanical properties and plastic deformation behavior of $La_{60}Al_{10}Ni_{10}Cu_{20}$, $Mg_{65}Cu_{25}Gd_{10}$, $Zr_{52.5}Al_{10}Ni_{10}Cu_{15}Be_{12.5}$, $Cu_{60}Zr_{20}Hf_{10}Ti_{10}$, and $Ni_{60}Nb_{37}Sn_3$ bulk metallic glasses have been studied using instrumented indentation. The hardness of these materials determined by nanoindentation are proportional to the yield strength with a slope near $K = 3.4$. Serrated flow was observed during nanoindentation in Mg-, Zr-, and Cu-based BMGs, wherein rapid loading rate suppressed and slower loading rate promoted prominent serrations. No distinct serrated flow was observed in Ni- and La-based BMGs at all the studied loading rates. The observations of the subsurface deformation zone proved that rapid loading rate leads to the increase of shear band density and the decrease of shear band thickness in Mg- and Zr-based BMGs. The large, widely spaced shear bands in the Mg-based BMG account for its high critical loading rate for the disappearance of serrated flow during indentation.

ACKNOWLEDGMENTS

The authors would like to acknowledge the financial support provided by National Nature Science Foundation of China (Grant Nos. 50101012, 10372103, and

10432050) and the Knowledge Innovation Program of Chinese Academy of Sciences.

REFERENCES

1 C C Hays, C P Kim, and W L Johnson: Microstructure controlled shear band pattern formation and enhanced plasticity of bulk metallic glasses containing in situ formed ductile phase dendrite dispersions *Phys Rev Lett* **84,** 2901 (2000)

2 G He, J Eckert, W Löser, and M Hagiwara: Composition dependence of the microstructure and the mechanical properties of nano/ultrafine-structured Ti–Cu–Ni–Sn–Nb alloys *Acta Mater* **52,** 3035 (2003)

3 K M Flores and R H Dauskardt: Fracture and deformation of bulk metallic glasses and their composites *Intermetallics* **12,** 1025 (2004)

4 H Ma, J Xu, and E Ma: Mg-based bulk metallic glass composites with plasticity and high strength *Appl Phys Lett* **83,** 2793 (2003)

5 C A Schuh and T G Nieh: A survey of instrumented indentation studies on metallic glasses *J Mater Res* **19,** 46 (2004)

6 A Inoue: Stabilization of metallic supercooled liquid and bulk amorphous alloys *Acta Mater* **48,** 279 (2000)

7 J Li, F Spaepen, and T C Hufnagel: Nanometre-scale defects in shear bands in a metallic glass *Philos Mag A* **82,** 2623 (2002)

8 T Sawa, Y Akiyama, A Shimamoto, and K Tanaka: Nanoindentation of a 10 nm thick thin film *J Mater Res* **14,** 2228 (1999)

9 A J Whitehead and T F Page: Nanoindentation studies of thin-film coated systems *Thin Solid Films* **220,** 277 (1992)

10 D Jang and M Atzmon: Grain-size dependence of plastic deformation in nanocrystalline Fe *J Appl Phys* **93,** 9282 (2003)

11 J J Kim, Y Choi, S Suresh, and A S Argon: Nanocrystallization during nanoindentation of a bulk amorphous metal alloy at room temperature *Science* **295,** 654 (2002)

12 C A Schuh and T G Nieh: A nanoindentation study of serrated flow in bulk metallic glasses *Acta Mater* **51,** 87 (2003)

13 T G Nieh, C Schuh, J Wadsworth, and Y Li: Strain rate-dependent deformation in bulk metallic glasses *Intermetallics* **10,** 1177 (2002)

14 W H Jiang and M Atzmon: Rate dependence of serrated flow in a metallic glass *J. Mater Res.* **18,** 755 (2003)

15 A L Greer and I T Walker: Transformations in primary crystallites in (Fe,Ni)-based metallic glasses *Mater Sci Forum* **77,** 386 (2002)

16 B C Wei, T H Zhang, W H Li, Y F Sun, Y Yu, and Y R Wang: Serrated plastic flow during nanoindentation in Nd-based bulk metallic glasses *Intermetallics* **12,** 1239 (2004)

17 C A Schuh, A C Lund, and T G Nieh: New regime homogeneous flow in the deformation map of metallic glasses: Elevated temperature nanoindentation experiments and mechanistic modeling *Acta Mater* **52,** 5879 (2004)

18 D Turnbull and M H Cohen: On the free-volume model of the liquid-glass transition *J Chem Phys* **52,** 3038 (1970)

19 A.S Argon: Plastic deformation in metallic glasses *Acta Metall* **27,** 47 (1979)

20 F Spaepan: A microscopic mechanism for steady state inhomogenous flow in metallic glasses *Acta Metall* **25,** 407 (1979)

21 A Pajares, L H Wei, B R Lawn, N P Padture, and C.C Berndt: Mechanical characterization of plasma sprayed ceramic coatings on metal substrates by contact testing *Mater Sci Eng* **A208,** 158 (1996)

22 W C Oliver and G M Pharr: An improved technique for determining hardness and elastic-modulus using load and displacement sensing indentation experiments *J Mater Res* **7,** 1564 (1992)

23 D Tabor: *The Hardness of Metals* (Oxford University Press, London, U K , 1951), p 37

24 J Basu, N Nagendra, Y Li, and U Ramamurty: Microstructure and mechanical properties of a partially crystallized La-based bulk metallic glass *Philos Mag* **83,** 1747 (2003)

25 N Q Chinh, J Gubicza, Zs Kovács, and J Lendvai: Depth-sensing deformation tests in studying plastic instabilities *J Mater Res* **19,** 31 (2004)

26 S Jana, U Ramamurty, K Chattopadhyay, and Y Kawamura: Subsurface deformation during Vickers indentation of bulk metallic glasses *Mater Sci Eng* **A375-377,** 1191 (2004)

27 U Ramamurty, S Jana, Y Kawamura, and K Chattopadhyay: Hardness and plastic deformation in a bulk metallic glass *Acta Mater* **53,** 705 (2005)

28 X K Xi, D Q Zhao, M X Pan, W H Wang, Y Wu, and J J Lewandowski: Fracture of brittle metallic glasses: brittleness or plasticity *Phys Rev Lett* **94,** 125510 (2005)